Electrical and physicochemical properties of some Ag2O-containing lithia iron silica phosphate glasses

ARTICLE *in* JOURNAL OF MATERIALS SCIENCE MATERIALS IN ELECTRONICS · JUNE 2011

Impact Factor: 1.57 · DOI: 10.1007/s10854-011-0561-0

3 AUTHORS:

Safeya Ibrahim
National Research Center, Egypt
14 PUBLICATIONS **53** CITATIONS
SEE PROFILE

Hussein Darwish
National Research Center, Egypt
43 PUBLICATIONS **239** CITATIONS
SEE PROFILE

Mohamed Gomaa
National Research Center, Egypt
29 PUBLICATIONS **169** CITATIONS
SEE PROFILE

Electrical and geochemical properties of tufa deposits as related to mineral composition in the South Western Desert, Egypt

2015 J. Geophys. Eng. 12 292

(http://iopscience.iop.org/1742-2140/12/3/292)

IOP Publishing Journal of Geophysics and Engineering
J. Geophys. Eng. **12** (2015) 292–302 doi:10.1088/1742-2132/12/3/292

Electrical and geochemical properties of tufa deposits as related to mineral composition in the South Western Desert, Egypt

Mohamed M Gomaa[1] **and Esmat A Abou El-Anwar**[2]

[1] National Research Center, Geophysical Sciences Department, Cairo, Egypt
[2] National Research Center, Geological Sciences Department, Cairo, Egypt

E-mail: mmmsgomaa@yahoo.com

Received 2 August 2014, revised 15 January 2015
Accepted for publication 18 February 2015
Published 31 March 2015

Abstract

The geochemical, petrographical, and electrical properties of rocks are essential to the investigation of the properties of minerals. In this paper we will try to present a study of the A. C. electrical properties of carbonate rock samples and their relation to petrographical and geochemical properties. Samples were collected from four formations from the Bir Dungul area, in the South Western Desert, Egypt.

The electrical properties of the samples were measured using a non-polarizing electrode, at room temperature (~28 °C), and at a relative atmospheric humidity of (~45%), in the frequency range from 42 Hz to 5 MHz. The changes in the electrical properties were argued to the change in mineral composition. Generally, the electrical properties of rocks are changed due to many factors e.g., grain size, mineral composition, grain shape and inter-granular relations between grains. The dielectric constant of samples decreases with frequency, and increases with conductor concentration. Also, the conductivity increases with an increase of continuous conductor paths between electrodes.

The petrographical and geochemical studies reveal that the deposition of the tufa deposits occurred in shallow lakes accompanied by a high water table, an alkaline spring recharge and significant vegetation cover. Diagenetically, tufa deposits were subjected to early and late diagenesis. Petrography and geochemistry studies indicated that the area of tufa deposits was deposited under the control of bacterial activity.

Geochemically, the Sr content indicates that the tufa deposits formed from dissolved bicarbonate under the control of microbes and bacterial activity.

Keywords: electrical properties, conductivity, dielectric constant, tufa, petrography, geochemistry

(Some figures may appear in colour only in the online journal)

1. Introduction

Tufa deposits were found overlying the Eocene Dungul Formation, the Paleocene Garra and Kurkur formations. The younger tufa deposits were deposited on a Kurkur Formation, while the older tufa was deposited on the Dungul Formation. During the Lower Eocene age, Southern Egypt was elevated until recent years. The oldest one was that of the Eocene Dungul Formation followed by the Paleocene Garra Formation and finally the younger surface of the Paleocene Kurkur Formation.

Tufa deposits are a porous or compacted type of calcium carbonate, which are deposited around springs and along river beds. They are often deposited around plants producing a

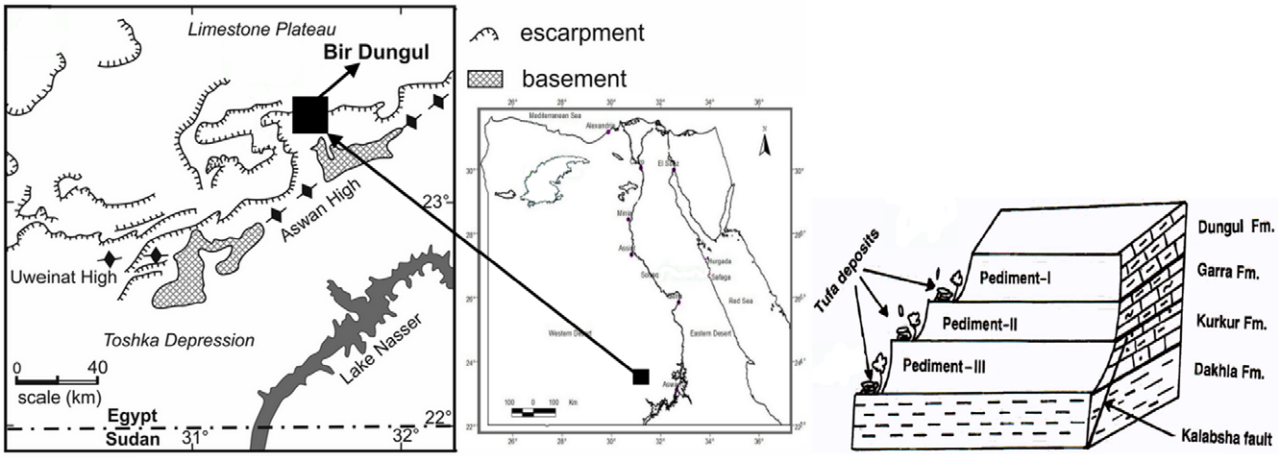

Figure 1. Geological and location map of the Bir Dungul area, South Western Desert, Egypt.

dendritic form (Pettijohn 1975). Tufa deposits are described as cool-water deposits of highly porous or spongy fresh-water carbonates, rich in micro-and macrophytic growth in leaves and woods (Pedley 1990, Banks *et al* 2012 and McBride *et al* 2012). In addition, chemically-precipitated non-marine limestone (calcite or aragonite) is deposited around springs (or lakes and rivers) and there is a terrestrial freshwater accumulation of calcium carbonate.

The Bir Dungul area lies between latitudes 23° 21′ 30″ – 23° 38′ 00″ N and longitudes 31° 21′ 30″ – 31° 35′ 00″ E, covering an area of some 7600 km^2 (figure 1).

The main goal of this paper is to shed more light on the relation the measured electrical properties (conductivity, dielectric constant and impedance as a function of frequency) have with petrography and the geochemical concentration of carbonate samples.

2. Geology

Issawi (1969) classified the exposed bedrock of tufa deposits in the Bir Dungel area from bottom to top as:

(a) **Dakhla Formation** (Maastrichtian to Paleocene): composed of shale beds with intercalated sandstone at the base and sandy shale limestone beds near the top. Some phosphate bands and lenses are developed at the base of the formation.

(b) **Kurkur Formation** (Early Paleocene): composed of sandstone-shale-limestone beds (deposited under the oscillation of shallow marine to protruding irrational facies.

(c) **Garra Formation** (Late Paleocene to Early Eocene): composed of gradational sequences of hard, gray to white calcareous shale- marl- chalky limestone beds. Flint bands, coral reefs, karst deposits, small caves and voids are clearly observed at the top of the sequence. Fossiliferous bands, iron oxy-hydroxide pockets and ferruginous encrusted zones are observed at the base of the sequence.

(d) **Dungul Formation** (Early Eocene): composed of alternating limestone and shale. The flint bands are confined to the lower and upper sections of the formation, especially with limestone beds.

(e) **Quaternary** deposits: in the Bir Dungul area are composed of many cycles of blown sand, silt and gravel. Karast deposits as well as flint sheets are found to cover local areas over the plateau surface. Tufa deposits have been laid down over the surface of the main plateau.

The measured A. C. electrical properties (conductivity, dielectric constant and impedance) of carbonate rocks could be of valuable interest for the investigation of hydrology methods (Olhoeft 1985), exploration methods and petrophysical applications. Physical and chemical interactions between grains in rocks play an important role in determining the electrical properties of rock samples (Sen 1981).

Generally, an increase of the conductive paths between the electrodes increases the conductivity and the dielectric constant (Gomaa 2008, Gomaa and Elsayed 2009). The electrical properties (conductivity, dielectric constant and impedance) depend on the charge density on the grains, grain shape, grain size, the conductor concentration and the properties of the electrolyte (conductivity and dielectric constant), and the measured frequency value (Gomaa 2004). With an increase of the insulator concentration or the insulator continuous paths, the dielectric constant value decreases. There is a critical percolation threshold with that increase of conductor concentration. At that percolation threshold the continuous paths begin to make contact with each other, forming conducting paths between the electrodes and accordingly more conductivity values are added (Knight and Endres 1990, Gomaa *et al* 2009).

3. Measurement of samples

The geochemical distribution of elements provides direct information on the depositional environment of the samples. Samples were measured using x-ray diffraction. The major

Table 1. The chemical analysis of the major and some trace elements of tufa deposits (Abou El-Anwar 2004) as well as the calculated carbon and the normative mineral composition).

Localities	Upper Plateau		Pediment I (Dungul Formation)			Pediment II (Garra Formation)		Pediment III (Kurkur Formation)		
Sample No.	**1**	**2**	**3**	**4**	**5**	**6**	**7**	**8**	**9**	**10**
SiO_2%	8.3	11.5	12.42	7.25	1.03	8.12	6.25	3.8	2.1	8.85
TiO_2%	0.04	0.05	0.08	0.15	0.1	0.15	0.04	0.05	0.07	0.08
Al_2O_3%	1.5	2.1	2.25	1.2	1.52	1.2	0.92	1.95	0.85	1.05
Fe_2O_3%	0.9	2.13	1.3	3.1	0.85	2.25	3.8	0.85	3.2	2.3
MgO%	1.85	2.2	2.65	0.6	4.1	0.5	1.62	4.8	2.05	5.32
CaO%	44.15	40.45	39.9	43.4	40.65	44.5	43.1	43.9	45.19	39.28
Na_2O%	0.3	0.4	1.08	0.5	0.29	0.35	0.58	0.4	0.35	1.5
K_2O%	0.15	0.32	0.25	0.18	0.24	0.18	0.28	0.24	0.32	0.64
P_2O_5	0.7	0.95	1.15	1.65	1.98	1.65	1.95	2.42	1.89	2.1
SO_3%	0.12	0.13	0.12	0.1	0.11	0.15	0.1	0.16	0.48	0.38
L. O. I.%	41.95	39.75	38.75	41.8	39.2	40.9	41.3	41.4	43.5	38.32
A. I. R.%	10.8	15.85	16.2	11.9	12.8	11.75	11.2	6.7	6.3	12.4
Sr ppm	300	350	300	350	300	200	400	200	350	300
Na* ppm	1100	1200	2100	1000	900	1300	1200	1000	1400	2300
$Sr/Ca(10)^{-3}$	0.7	1.42	0.75	0.7	0.81	0.74	0.93	0.46	0.78	0.76
$Mg/Ca(10)^{-2}$	4.2	5.4	6.6	1.4	10.1	1.1	3.7	10.7	4.5	13.5
Cal. C	11.45	10.85	10.58	11.41	10.7	11.16	11.27	11.3	11.87	10.46
N. Calcite	75.1	73.6	69.88	86.1	65.62	85.52	81.15	68.39	82.54	55.96
N. Dolomite	12.65	12.09	14.49	3.37	22.54	2.73	9.04	24.76	11.67	26.56
N. Halite	0.65	0.73	1.86	0.95	0.51	0.63	1.05	0.71	0.63	2.44
N. Gypsum	0.26	0.21	0.21	0.06	0.15	1.26	0.1	0.2	0.63	0.49
N. Hem./Geo.	0.39	0.73	0.47	1.11	0.31	0.84	1.31	0.3	1.15	0.72

Note: *L. O. I.*, loss of ignition (the total CO_2 in the bulk sample); *A. I. R.*, acid insoluble residue; *Na**, Co-precipitated sodium; *Cal. C*, calculated total carbon form CO_2 of the bulk samples; *N. Calcite*, normative Calcite; *N. Dolomite*, normative dolomite; *N. Halite*, normative halite; *N. Gypsum*, normative gypsum; *N. Hem./Geo.*, normative hematite/geothite.

and trace elements of samples were analyzed by XRF. The instrument of x-ray fluorescence was (PW-1050/180) jointed to an x-ray powder generator (PW-1140/90). The x-ray tube was a Cu-target model (PW-2233/20) fitted with a Ni filter. The calculated normative mineral composition is shown in table 1.

The geometry of the samples for electrical measurements was chosen to reduce errors due to stray capacitance. A Hioki 3522- 50 LCR Hitester Impedance Analyzer was used to measure the electrical properties (dielectric constant, conductivity, impedance). The sample edges were polished to be parallel. The samples cover all the formations in the studied area. The electrical properties were measured in the frequency range from 42 Hz up to 100 kHz, using non-polarizing electrodes ($Cu/CuSO_4$) at an oscillation amplitude of 1 v (Gomaa 2009).

The electrical properties of the samples may be measured in either the series or in parallel configuration. The parameters were measured using parallel capacitance and conductance (C_p and G_p) and series impedance Z at different frequencies. The complex relative dielectric constant is $\varepsilon^* = \varepsilon' - i\varepsilon''$, where, $\varepsilon' = C_p d/\varepsilon_0 A$, is the real part of the complex relative dielectric constant before correction and the imaginary part of the complex relative dielectric constant is $\varepsilon'' = G_p d/\omega\varepsilon_0 A$, where A is the cross-sectional area of the sample, d is the sample thickness, $\varepsilon_0 = 8.85 \times 10^{-12}$ is the free space permittivity and ω is the angular frequency. The real conductivity is $\sigma' = G_p d/A = \varepsilon'' \omega\varepsilon_0$.

The electrical properties were measured in an isolated chamber at relative atmospheric humidity of (~45%) at room temperature (~28 °C) (desiccator) (Gomaa and Alikaj 2010, Gomaa 2011). A correction due to fringing for the capacitance can be used through the following formula (Chew and Kong 1980):

$$C \approx \frac{a^2\pi\varepsilon_r\varepsilon_0}{d}\left\{1 + \frac{2d}{\pi\varepsilon_r a}\left[\ln\left(\frac{a}{2d}\right) + (1.41\varepsilon_r + 1.77) + \frac{d}{a}(0.268\varepsilon_r + 1.65)\right]\right\} \quad (1)$$

where a is the radius of the disk and ε_r is the relative permittivity. The electrode impedance was found to be of the order of (15 − J 0.1) Ω within the used frequency range and it was removed from the measurements (Gomaa 2004).

4. Results and discussion

4.1. Petrography

The deposition environment of the Tufa deposits occurs at shallow lakes at wet and warm conditions. It is suggested to be accompanied by a high water table and by the alkaline spring recharge of considerable vegetation cover (Abou El-Anwar 2004, Domínguez-Villar *et al* 2012). From a petrographical point of view, Tufa deposits are classified into four microfacies, according to their redundancy in the following:

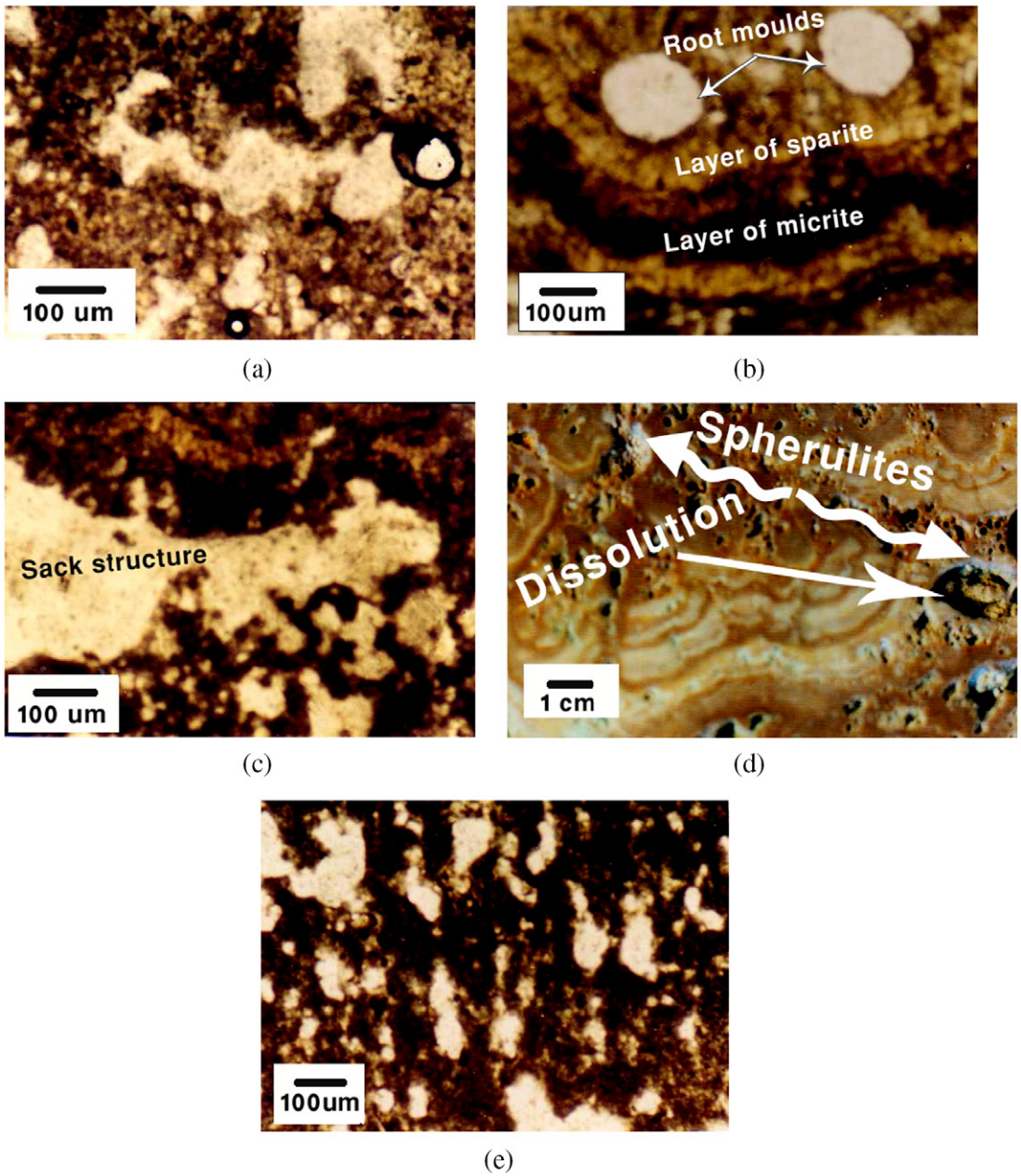

Figure 2. The petrographical features of the studied samples. (*a*) Porous bioclastic tufa showing micritic calcite septa that surround and interconnect irregular voids. (*b*) Porous bioclastic tufa showing tabular voids of root moulds surrounded by alternating layers of micrite and sparite as aggrading neomorphism. (*c*) Cellular algal tufa showing sack-like structure. (*d*) Stromatolite algal tufa separated between porous and hard massive tufa. Note: spherulites grains and the dissolution effect. (*e*) Stromatolite algal tufa showing cyanobacteria shrubs.

4.1.1. Porous bioclastic tufa. Are the most abundant microfacies in the studied deposits. They are highly fossiliferous with the remains of roots, stems, trunks and leaves as well as abundant stalk moulds. Several organo-sedimentary structures are documented in samples of these lithofacies, either in hand-specimens or in thin-sections (figure 2(*a*)). The main diagnostic features of organo-sedimentary accretion and microbialites are laminations, typical microfabrics and remnants of fossilized microbes (Tribovillard *et al* 2012). Root moulds are tabular voids that consist of alternating layers of micrite and sparite surrounding the plant-like pipe, which show aggrading neomorphism (figure 2(*b*)). The micritized sheath covers the root casts and produces characteristic rhizocretions, which are related to root growth and decay (Adams and Mackenzie 1998). The micritic envelope represents a calcareous sheath around the root casts and leaves.

4.1.2. Cellular algal tufa. It consists of a porous rock (figure 2(*c*)) composed of an irregular three-dimensional network of thin micritic encrusting sheaths. Microscopically, some samples contain sack-like structures that appear as laterally connected sacks and hemispheres (figure 2(*c*)). The sacks may represent algal structures and suggest the possibility that some septa are inorganic precipitates on organic mats (Bouougri *et al* 2012). Dissolution is the most important diagenetic feature that affects microfacies (25–35%), followed by a micritic

envelope and recrystallization formed by the action of meteoric waters in late diagenesis (Abou El-Anwar 2011). Cellular algal tufa may be deposited in stagnant ponds at the close of the rainy season.

4.1.3. Stromatolite algal tufa. Are laminated rocks interpreted as filamentous blue-green algae. They occur as a separate thin crust between porous tufa and fresh water limestone or massive tufa (figure 2(*d*)). Microscopically, stromatolite algal tufa is composed of calcified filaments embedded in a micritic matrix. Figure 2(*e*) shows the cyanobacteria shrubs in stromatolite tufa, which are very important in the production of the laminated carbonate sediments known as stromatolites (Bouougri *et al* 2012). The microfacies display the same diagenetic features of porous and cellular tufa and contain some spherulites (figure 2(*d*)). This indicates that the carbonate was rapidly precipitated during flash boiling in the spring orifice and that the water was cooled to around 50 °C (Brock 1976). On the other hand, iron oxy-hydroxide was deposited at a late stage (Chaojun *et al* 2010).

4.1.4. Hard massive tufa. Are represented by dense, hard yellowish tufa cuttings through the porous and algal Tufa. Massive carbonate mineral formation was largely controlled by microbial metabolism (Martinez *et al* 2010) and linked to algal and coral growth (Ries 2010). Furthermore, it is distinguished by some nodules of chert. It is characterized by organo-sedimentary structures and calcified stems. Microscopically, it consists of a micritic matrix surrounding the small voids, indicating that the early diagenetic calcification took place during the decay of the plant. The secondary porosity (8%), which is due to the effect of dissolution, is represented by small groves.

4.2. Mineralogy and geochemistry

Mineralogical investigation by XRD analysis (figure 3) reveals that tufa is composed mainly of calcite with minor amounts of clay minerals, halite, gypsum, dolomite and quartz (Abou El-Anwar 2004). Kouzana *et al* (2010) indicated that the boundary between freshwater and saltwater is an ideal application for resistivity surveys due to the high contrast of electrical conductivity between salt and fresh water.

Table 1 shows the chemical analysis and the major elements of tufa deposits. In the chemical analysis, the sand grains or clay minerals are represented by SiO_2, which are not represented in the main components of the carbonate rocks. The SiO_2 content in the samples ranges from 2.10 to 12.42%. There are positive correlation coefficients between SiO_2 with acid insoluble residue and Al_2O_3 which are 0.96 and 0.56, respectively. This indicates that quartz is the main quotient of silica, while clays are subsidiary. This may be the main reason for the low values of conductivity in the samples.

Fe_2O_3 is variably distributed in the samples (0.85 to 3.80%). Abrajevitch *et al* (2009) indicates that iron 'hematite/gotheite' is related to the supergene alteration. The solids dissolved in acid–saline groundwater give high concentrations of Fe. Furthermore, the evaporation of water concentrates minor soluble salts (gypsum and some halite) on the grain surfaces which leads to the formation of a line within the porous sediments by the hydrostatic forces around the salt-lake (Long *et al* 2009 and McLaren and Wallace 2010). The positive correlation between Fe_2O_3 and Sr (0.39) indicates that iron may scavenge and uptake Sr (Abou El-Anwar 2012). Evidence for the input of detrital material is derived from the presence of Ti, Al, K and Fe related to quartz and clay minerals (Currás *et al* 2012). Low Sr/Ca $(10)^{-3}$ indicates that tufa was probably deposited from bicarbonate-rich water and precipitated from fresh water (<1% salinity) (Mahmoud *et al* 2002, table 1).

Kurkur Formation (Samples No. 8, 9 and 10) has the highest normative mineral composition of dolomite and halite (table 1). Sample 10 shows a high percentage of normative composition of dolomite and halite as well as a moderate value of normative calcite. Sample No. 8 has the lowest recorded percentage of gypsum and hematite. This may be the main reason for the high value of conductivity in sample 10 and the low value of conductivity in sample 8.

Garra Formation (Samples No. 6 and 7) is characterized by iron oxy-hydroxide pockets and ferreginous encrustation. It has the highest value of gypsum (1.26 %, sample No. 6) and mineral composition of hematite (table 1). Sample 7 shows the highest normative mineral composition of hematite (1.31%). Abrajevitch *et al* (2009) demonstrate that a statistical analysis of the isothermal remnant magnetization curves provides an adequate estimate of the content of goethite and hematite in the sediments. Furthermore, variations in the 'detrital' at the same stratigraphic level, suggest that a change in magnetic mineral content reflects a change in the degree of diagenetic alteration. Sample No. 6 has the highest recorded normative mineral composition of gypsum (1.26%) in addition to a very low normative composition of dolomite (2.73%). Sample 7 has the lowest value of dielectric constant (figure 6). This may be due to the relatively large distances of the insulator grains between the conductor grains.

Dungul Formation and Upper Plateau (Samples No. 1–5). The samples have nearly the same average normative composition of dolomite (except sample No. 5), hematite (except sample No. 4) and gypsum (table 1). Sample No. 5 shows the highest value of normative dolomite. Sample No. 4 is distinguished by the highest value of normative calcite and hematite and the lowest value of normative dolomite and gypsum (table 1). Sample No. 3 has the highest value of halite (table 1).

4.3. Electric

Figure 4 shows the change of conductivity with frequency. The conductivity increases with the increase of frequency and with the increase of total conductor concentration which leads to the increase of continuous conduction paths in the samples. Figure 5 shows the change of the dielectric constant with frequency. The dielectric constant decreases with an increase of frequency and increases with the increase of total conductor concentration in the sample up to a certain

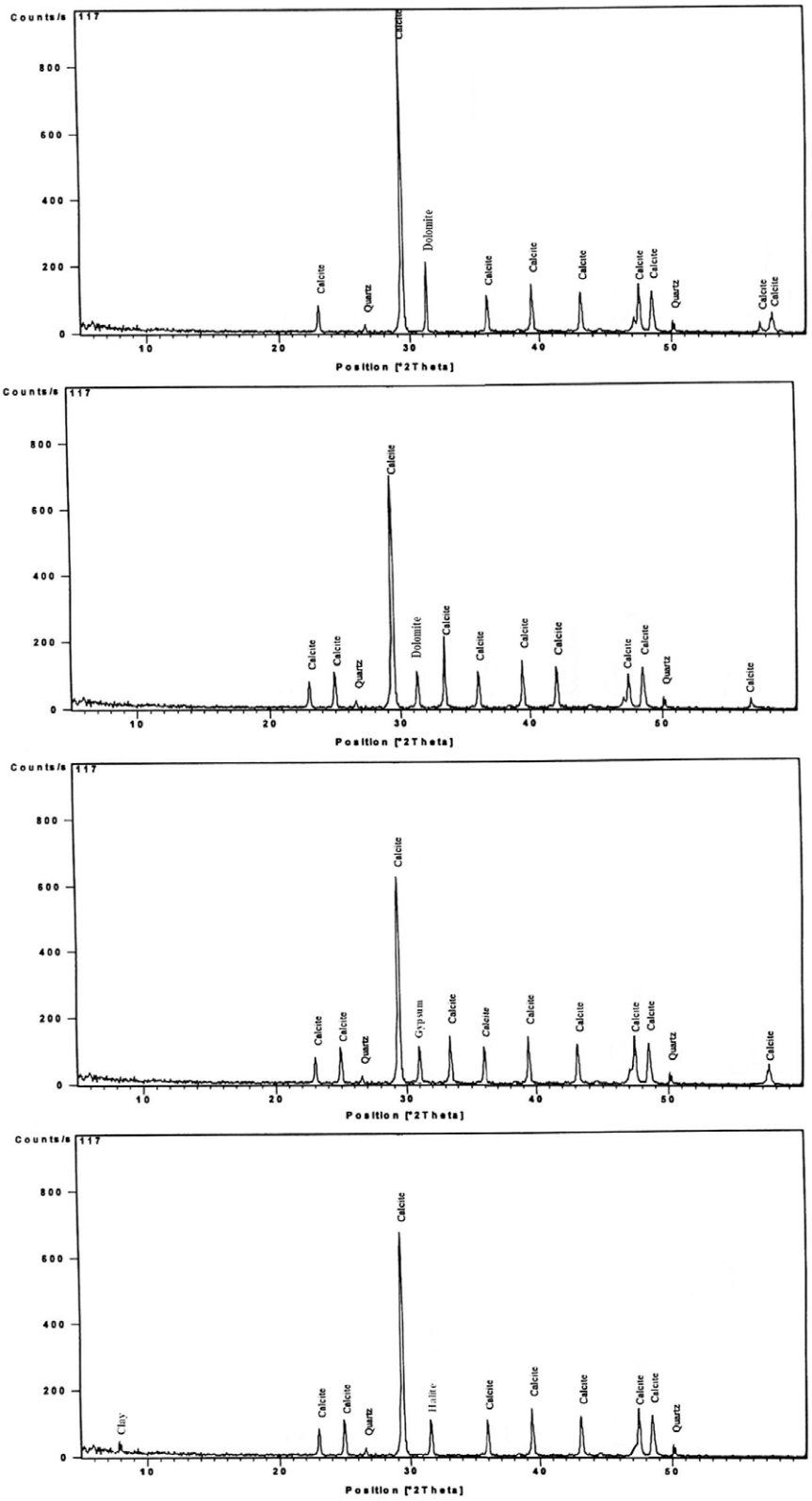

Figure 3. The XRD features of the studied samples. From top to bottom Upper Plateau, Dungul Formation, Garra Formation, Kurkur Formation.

limit (percolation threshold) (Shaltout *et al* 2012). Above the percolation threshold the dielectric constant decreases with an increase of the total conductor concentration in the samples. This is due to the blocking of the conductor continuous paths in the samples. Figure 6 shows the variation of the complex impedance of the samples. The measured data of the complex impedance nearly show an arc. With the increase of the conductor conduction paths this arc is contracted to be a part of a semicircle. The conductor conduction paths are the summation of the different conductor concentrations in the sample.

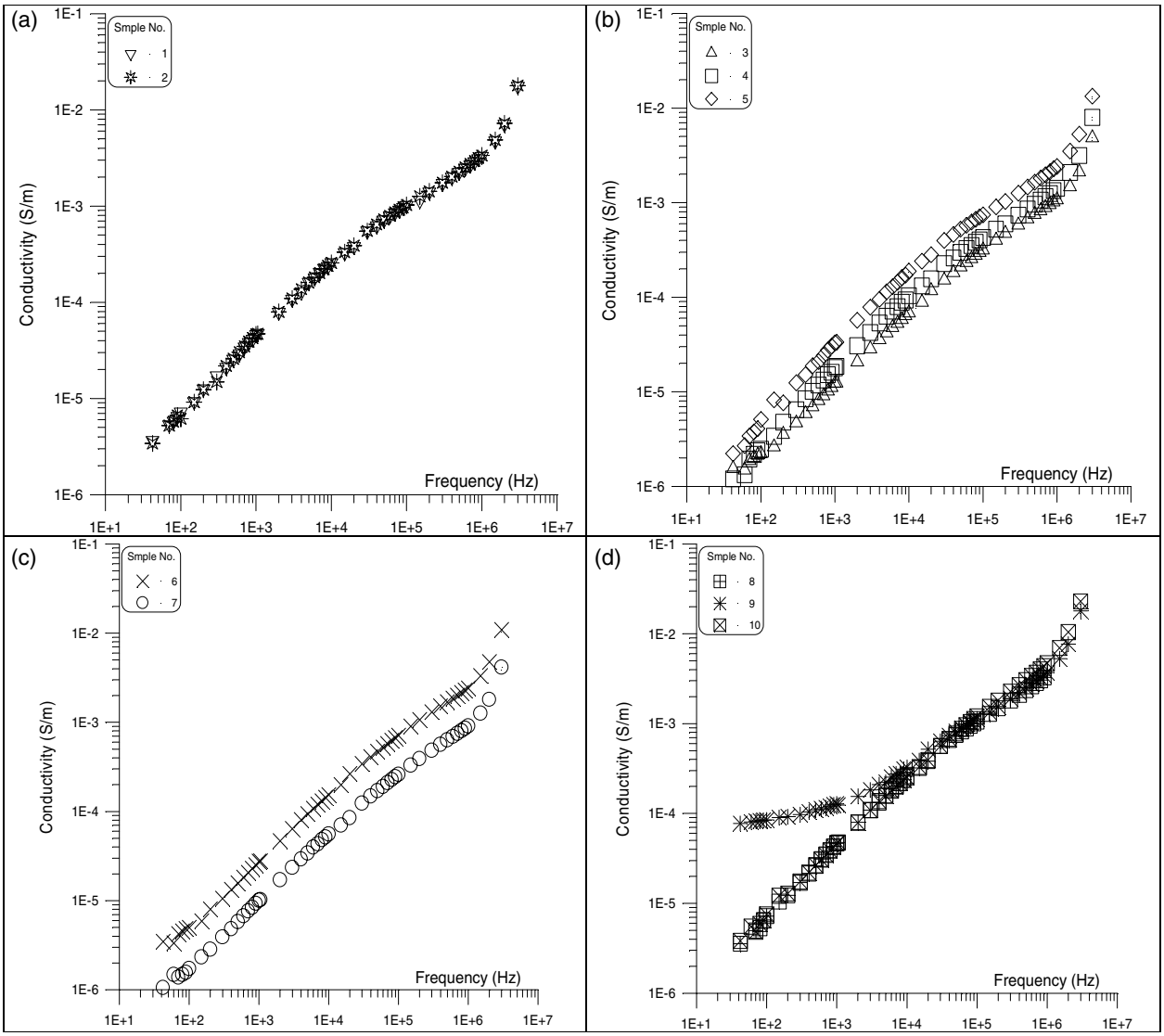

Figure 4. The variation of the conductivity with frequency. (*a*) Upper Plateau (No. 1, 2), (*b*) Dungul Formation (No. 3-5), (*c*) Garra Formation (No. 6, 7), (*d*) Kurkur Formation (No. 8-10). Conductor concentrations for samples from 1 to 10 are as follows (11.84, 11.58, 11.05, 12.52, 11.01, 12, 12.58, 11.6, 13.02 and 11.18).

The real and imaginary impedance of the samples decreases with an increase of the conductor conduction paths between electrodes (different conductor concentration). The elements that are assumed to be insulators are normative calcite, normative dolomite, normative halite and normative gypsum, while the elements that are assumed to be conductors are calculated carbon and normative hematite/geothite (table 1).

4.3.1. Upper Plateau (Samples No. 1 and 2, figure 2(b) and (c). This group is relatively more insulating than the other three groups. Conductivity shows a general trend of increasing with frequency, while the general trend of the dielectric constant shows a decrease with frequency (figures 2(*c*), 4, and table 1). It is noticed that the behavior of the two samples (1 and 2) match each other. This may be due to the comparable conductor concentration in the two samples. This is a good indicator that the samples all over the area are homogeneous and these samples are a good representative of the formation. Most of the conducting materials in these samples are dispersed and coated with the insulating materials (figures 2(*b*) and (*c*)) and that is the reason why they are more insulating than the other three groups.

A relatively high value of the dielectric constant in the samples may be due to the presence of conducting grains coated by insulator materials or may be attributed to the small pores between the grains in the samples.

4.3.2. Dungul formation (Samples No. 3, 4 and 5). This group is more conductive than the previous group (upper plateau). Generally, the conductivity increases from sample 4 to 5 to 6 due to the increase of the concentration of the conducting elements and the decrease of the insulating elements. In addition, the dielectric constant increases from sample 4 to 5 to 6 due to the increase of the concentration of the conducting material that may be attributed to the presence of gaps from insulating materials between the conducting grains. With the increase of the conducting material, the insulating gaps decrease and the dielectric constant increases.

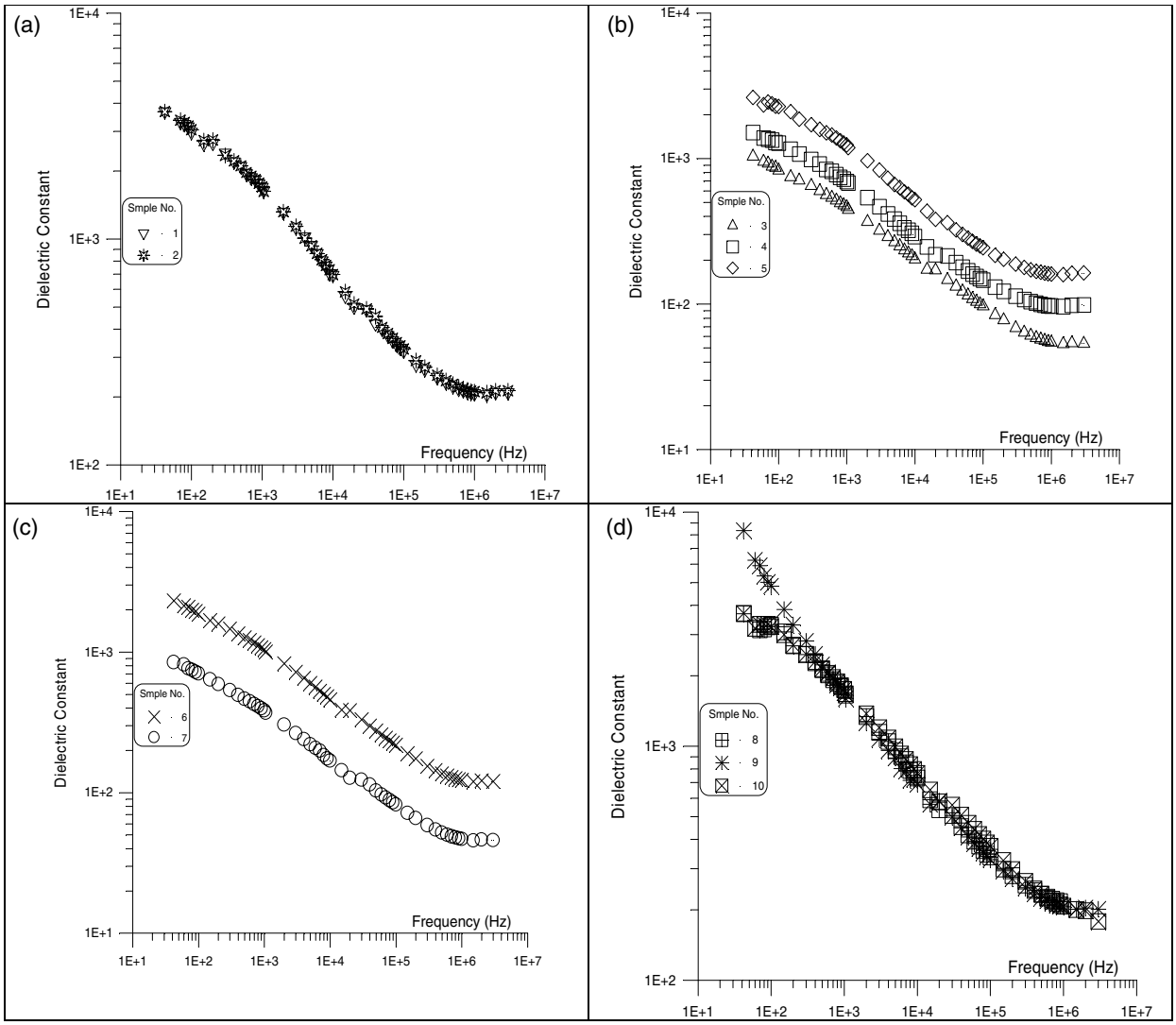

Figure 5. The variation of the dielectric constant with frequency. (*a*) Upper Plateau (No. 1, 2), (*b*) Dungul Formation (No. 3-5), (*c*) Garra Formation (No. 6, 7), (*d*) Kurkur Formation (No. 8-10). Conductor concentrations for samples from 1 to 10 are as follows (11.84, 11.58, 11.05, 12.52, 11.01, 12, 12.58, 11.6, 13.02 and 11.18).

4.3.3. Garra formation (Samples No. 6 and 7). This group generally has a moderate conductivity and dielectric constant. The conductivity decreases from sample 7 to 6 and the dielectric constant increases with an increase of the percentage of insulator concentration and with frequency (figures 4–6). The conductivity increases with the increase of the concentration of the conductor that is attributed to the increase of paths of conducting grains, between the electrodes. Furthermore, the dielectric constant decreases with the decrease of concentration of the conductor due to an increase of distances and of insulator air gaps between conducting grains. In these samples most of the conducting elements are dispersed between insulator elements. That is clear from the relatively low value of the conductivity in the presence of relatively high conductor concentration. Sample 7 has the lowest value of dielectric constant (figure 6), which may be due to the relatively large distances of the insulator grains between the conductor grains.

4.3.4. Kurkur formation (Samples No. 8, 9 and 10). These samples show a tendency to be more conductive than the other three groups, especially sample 9. This sample has the highest value of conductivity and dielectric constant. The high values of the dielectric constant may be attributed to the presence of relatively smaller grains of insulator between the conducting grains, while the high values of conductivity may be due to the presence of more conducting paths between the electrodes. Furthermore, sample 9 shows a high percentage of calcite and hematite, while sample 8 has the lowest recorded percentage of gypsum and hematite. This may be the main reason for the high value of conductivity in sample 9 and the low value of conductivity in sample 8.

Figure 4 shows the variation of conductivity with frequency. Generally, conductivity increases with an increase of frequency. The abrupt variation in conductivity shown in sample 9 may be due to the presence of a direct current continuous path (DC) (Efros and Shklovskii 1976). We can also see from samples 6 to 9 that the conductivity increases with conductor concentration (Levitskaya and Sternberg 1996). One slope can be noticed with a frequency for all the curves (except sample 9). The conductivity is low at low

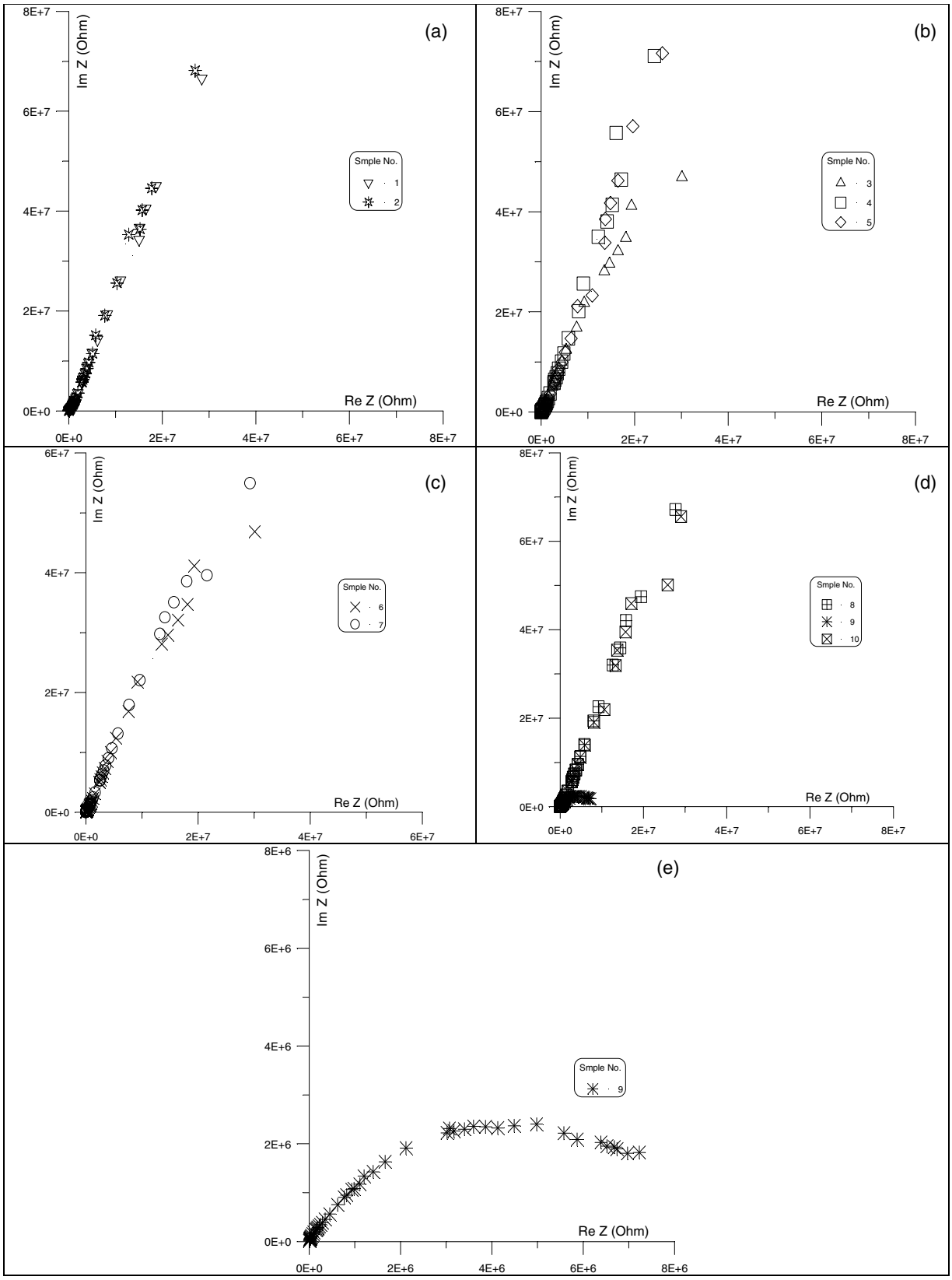

Figure 6. The complex impedance plane representation of the samples. (*a*) Upper Plateau (No. 1, 2), (*b*) Dungul Formation (No. 3-5), (*c*) Garra Formation (No. 6, 7), (*d*) Kurkur Formation (No. 8-10). Conductor concentrations for samples from 1 to 10 are as follows (11.84, 11.58, 11.05, 12.52, 11.01, 12, 12.58, 11.6, 451 13.02 and 11.18).

total conductor concentration and at low frequency. At higher frequencies and higher total conductor concentration, more continuous conductor paths exist between grains which lead to an increase of conductivity values (Knight 1983, Levitskaya

and Sternberg 2000). The increase of frequency motivates particles to overcome barriers between energy levels to form continuous conductor paths between the grains and accordingly the conductivity increases (Jonscher 1999).

The gradual increase in the dielectric constant with increasing total conductor concentration may be attributed to the decrease of the air space distance (or insulator elements) between the grains that behave as a capacitor, especially for low total conductor concentration. The capacitance gradually increases as the total conductor concentration increases (Chelidze and Gueguen 1999, Chelidze *et al* 1999, Jonscher 1999).

Figure 6 shows the complex impedance plane variation of samples with different concentrations. Generally, for low concentrations of a conductor an arc in the impedance plane can be seen and this arc is contracted to the part of the semicircle with an increase of conductor concentrations. This arc may be contracted to a semicircle at the higher conductor concentrations (Grant 1958). Sample 7 and 9 may be compared to each other; they show an arc and a depressed semicircle (or it may be a semicircle), respectively. The increase in real impedance may be attributed to an increase of the continuous conductor paths between electrodes.

Generally, the conductivity increases with the increase in the total conductor concentration, which may be attributed to the increase of the relatively conducting paths between the electrodes. The conductivity increases sharply, at low conductor concentrations, and at higher conductor concentrations it begins to saturate as the conductivity reaches its maximum value. At high frequencies (1 MHz) the conductivity shows a value of the order of $10^{-2}\,S\,m^{-1}$ (figure 4).

Generally, the dielectric constant increases with an increase of total conductor concentration, which may be attributed to a decrease of distances between the relatively more conductive grains. This occurs directly due to the increase of the relatively more conductive concentrations (Knight and Nur 1987). The distances between the relatively more conductive grains decreases until it vanishes and the first continuous conductor path begins to be formed, then with the increase of relatively conducting concentrations the dielectric constant begins to decrease again (this is not seen in our group of samples). This is what is called the critical concentration. The dielectric constant increases for the relatively higher conductor concentrations to reach a value of 200 (samples 1, 4, 9 and 7).

With the changes in texture (grain size, grain shape, concentration and porosity) from one sample to another, the curves changed, even if they have the same concentration, because the texture is not the same (Abou El-Anwar and Gomaa 2013).

5. Conclusion

Electrical, petrographical and geochemical discussions and interpretations were made in order to explore the relation between geochemical composition of measured samples (carbonates that contain clays and quartz grains) and texture. Electrical properties were analyzed using a non-polarizing electrode at room temperature (~28 °C) and at a relative atmospheric humidity of (~45%) in the frequency range from 42 Hz up to 1 MHz.

Tufa deposits were formed in shallow lakes at close proximity to the spring orifice, where physicochemical and biological processes dominate. Theses deposits consisted of four microfacies and were subjected to early and late diagenesis processes. The low Sr/Ca (10^{-3}) indicates that the tufa deposits were deposited from bicarbonate water and precipitated from fresh water. The high concentrations of MgO, Fe_2O_3 and P_2O_5 were attributed to hot water springs passing through the Dakhla (shale) Formation and are interpreted to be the result of bacterially induced precipitation.

The Kurkur Formation recorded the highest values of normative dolomite and halite. The Dungul Formation recorded the highest value of normative calcite. The Garra Formation recorded the highest values of gypsum and hematite.

The electrical responses of the individual components of the samples (texture) change when the combinations of the components are changed and this may be due to interactions on their surfaces. Furthermore, these values are influenced by the concentrations of conductive and/or insulating particles in the samples especially at low frequencies. The dielectric constant and conductivity increases with the increase of the relative conductor concentration. The dielectric constant decreases with a frequency increase while conductivity increases with a frequency increase. The dielectric properties may be attributed to an increase of the conductive concentration. As the conductive clustering materials are increased and the thickness of the insulating gaps between conductive clusters decreases, an increase in the dielectric constant of the samples is shown.

Conductors (calculated carbon and normative hematite/geothite) and insulators (normative calcite, normative dolomite, normative halite and normative gypsum) combine together to give the net final degree of conduction or insulation in the samples.

References

Abou El-Anwar E A 2004 Petrography, geochemistry and genesis of Tufa deposits of Bir Dungul area, south western desert, Egypt *Sedimentol. Egypt* **12** 131–47

Abou El-Anwar E A 2011 Petrographical, geochemical and diagenetic studies of the Middle Eocene carbonates, Mokattam Formation of Darb El-Fayium area *Int. Conf. on Geological and Engineering* (*Paris, France, 24–26 August 2011*) vol 80, pp 1315–25

Abou El-Anwar E A 2012 Contribution to the composition and origin of the reef Terraces in Ras Mohamed, Sharm El-Sheikh Coast, Southern Sinai *Egypt. Geol. Soc. Egypt* **56** 33–48

Abou El-Anwar E and Gomaa M M 2013 Electrical properties and geochemistry of carbonate rocks from the Qasr El-Sagha formation, El-Faiyum, Egypt *Geophys. Prospect.* **61** 630–44

Abrajevitch A, Van R and Rea D K 2009 Variations in relative abundances of goethite and hematite in Bengal Fan sediments: climatic versus diagenetic signals *Marine Geol.* **267** 191–206

Adams A E and Mackenzie W S 1998 *A Color Atlas of Carbonate Sediments and Rocks Under the Microscope* (London: Manson) p179

Banks V, Jones P, Low D, Lee J, Rushton J and Ellis M 2012 Review of tufa deposition and palaeohydrological conditions in the White Peak, Derbyshire, UK: implications for Quaternary landscape evolution *Proc. Geol. Assoc.* **123** 117–29

Bouougri E H, Porada H, Reitner J and Gerdes G 2012 Preface: introduction to the special issue 'Signatures of microbes and microbial mats and the sedimentary record' *Sediment. Geol.* **336** 51–63

Brock T D 1976 Environmental microbiology of living stromatolites ed M R Walter *Stromatolites* (New York: Elsevier) pp 141–8

Chaojun F, Hongjie X, DirkSchulze-Makuch B and Ackley S 2010 A formation mechanism for hematite-rich spherules on Mars *Planetary Space Sci.* **58** 401–10

Chelidze T and Gueguen Y 1999 Electrical spectroscopy of porous rocks: a review -I. Theoretical models *Geophys. J. Int.* **137** 1–15

Chelidze T, Gueguen Y and Ruffet C 1999 Electrical spectroscopy of porous rocks: a review -II. Experimental results and interpretation *Geophys. J. Int.* **137** 16–34

Chew W C and Kong J A 1980 Effects of fringing fields on the capacitance of circular microstrip disk *IEEE Trans. Microwave Theory Tech.* **MTT-28** 98–104

Currás A, Zamora L, Reed J M, García-Soto E, Ferrero S, Armengol X, Mezquita-Joanes F, Marqués M A, Riera S and Julià R 2012 Climate change and human impact in central Spain during Roman times: high-resolution multi-proxy analysis of a tufa lake record (Somolinos, 1280 m asl) *CATENA* **89** 31–53

Domínguez-Villar D, Vázquez-Navarro J and Carrasco R 2012 Mid-Holocene erosive episodes in tufa deposits from Trabaque Canyon, central Spain, as a result of abrupt arid climate transitions *Geomorphology* **161–162** 15–25

Efros A L and Shklovskii B I 1976 Critical behavior of conductivity and dielectric constant near the metal–non-metal transition threshold *Phys. Status Solidi* **76** 475–89

Gomaa M M and Alikaj P 2010 Effect of electrode contact impedance on ac electrical properties of wet hematite sample *Marine Geophys. Res.* **30** 265–76

Gomaa M M 2004 Induced polarization Study on iron ore bearing rock samples *PhD Thesis* Cairo University, Egypt

Gomaa M M 2008 Relation between electric properties and water saturation for hematitic sandstone with frequency *Ann. Geophys.* **51** 801–11

Gomaa M M 2009 Saturation effect on electrical properties of hematitic sandstone in the audio frequency range using non-polarizing electrodes *Geophys. Prospect.* **57** 1091–100

Gomaa M M 2011 Horizons in earth science research, chapter 2, factors affecting electrical properties of sedimentary rocks *Horizons in Earth Science Research* ed B Veress and J Szigethy, vol 6 (Hauppauge, NY: Nova Science) pp 83–146

Gomaa M M and Elsayed M 2009 Thermal effect of Magma intrusion on electrical properties of magnetic rocks from Hamamat Sediments, NE Desert, Egypt *Geophys. Prospect.* **57** 141–9

Gomaa M M, Shaltout A and Boshta M 2009 Electrical properties and mineralogical investigation of Egyptian iron ore deposits *Mater. Chem. Phys.* **114** 313–8

Grant F A 1958 Use of complex conductivity in the representation of dielectric phenomena *J. Appl. Phys.* **29** 76–80

Issawi B 1969 The geology of Kurkur–Dungul area *Geol. Surv. Egypt* **46** 1–101

Jonscher A 1999 Dielectric relaxation in solids *J. Phys. D: Appl. Phys.* **32** R57–70

Knight R J and Endres A L 1990 A new concept in modeling the dielectric response of sandstones: defining a wetted rock and bulk water system *Geophysics* **55** 586–94

Knight R J and Nur A 1987 The dielectric constant of sandstones, 50 kHz to 4 MHz *Geophysics* **52** 644–54

Knight R 1983 The use of complex plane plots in studying the electrical response of rocks *J. Geomag. Geoelectr.* **35** 767–76

Kouzana L, Benassi R, Ben Mammoua A and Sfar Felfoul M 2010 Geophysical and hydrochemical study of the seawater intrusion in Mediterranean semi arid zones. Case of the Korba coastal aquifer (Cap-Bon, Tunisia) *J. African Earth Sci.* **58** 242–54

Levitskaya M T and Sternberg K B 1996 Polarization processes in rocks 1. Complex dielectric permittivity method *Radio Sci.* **31** 755–79

Levitskaya T M and Sternberg B K 2000 Application of lumped-circuit method to studying soils at frequencies from 1 kHz to 1 GHz *Radio Sci.* **35** 371–83

Long D T, Lyons W B and Hines M E 2009 Influence of hydrogeology, microbiology and landscape history on the geochemistry of acid hypersaline waters *Applied Geochemistry* ed N W Victoria, vol 24 (Amsterdam: Elsevier) pp 285–96

Mahmoud A A, El-Gohary A and Abou El-Anwar E A 2002 Geology of quaternary tufa deposits North–East of the Dakhla oasis, Western Desert, Egypt *Sedimentology* **10** 89–100

Martinez R E, Gardés E, Pokrovsky O S, Schott J and Oelkers E H 2010 Do photosynthetic bacteria have a protective mechanism against carbonate precipitation at their surfaces? *Geochim. Cosmochim. Acta* **74** 1329–37

McBride J, Guthrie W, Faust D and Nelson S 2012 A structural study of thermal tufas using ground-penetrating radar *J. Appl. Geophys.* **81** 38–47

McLaren S and Wallace M 2010 Plio-pleistocene climate change and the onset of aridity in southeastern Australia *Global Planetary Change* **71** 55–75

Olhoeft G R 1985 Low frequency electrical properties *Geophysics* **50** 2492–503

Pedley H M 1990 Classification and environmental modles of cool fresh water *Tufas Sediment. Geol.* **68** 143–54

Pettijohn E 1975 *Sedimentary Rocks* (New York: Harper and Raw) p 688

Ries J B 2010 Review: geological and experimental evidence for secular variation in seawater Mg/Ca (calcite–aragonite seas) and its effects on marine biological calcification *Biogeosciences* **7** 2795–849

Sen P N 1981 Dielectric anomaly in inhomogeneous materials with application to sedimentary rocks *Appl. Phys. Lett.* **39** 667–8

Shaltout A A, Gomaa M M and Wahbe M 2012 Utilization of standard-less analysis algorithms using WDXRF and XRD for Egyptian iron ores identification *X-Ray Spectrom.* **41** 355–62

Tribovillard N, Sansjofre P, Ader M, Trentesaux A, Averbuch O and Barbecot F 2012 Early diagenetic carbonate bed formation at the sediment–water interface triggered by synsedimentary faults *Chem. Geol.* **300–1** 1–13